Multibody Syst Dyn
https://doi.org/10.1007/s11044-020-09761-x

Tip-trajectory tracking control of a deployable cable-driven robot via output redefinition

S.A. Khalilpour[1] · R. Khorrambakht[1] · H. Damirchi[1] · H.D. Taghirad[1] · P. Cardou[2]

Received: 2 February 2020 / Accepted: 16 October 2020

Abstract Large-scale deployable cable-driven robots face a lack of kinematic precision, and the cable dynamics impose considerable challenges in terms of controller design. The problem's complexity increases because a deployable robot may not exploit expensive and highly accurate of measurement devices. Thus, it is necessary to efficiently combine the set of measurements available through low-cost sensors to track the end-effector's position and reduce the oscillations. This paper's main contribution is to propose a novel feedback method for fusing the vision and joint kinematic sensors for achieving suitable tracking performance. To this end, the dynamic formulation of a large-scale deployable cable-driven robot has been derived considering a lumped mass model for the cables. Based on this model, it is then shown that the stability conditions are satisfied through a suitable combination of sensory data incorporated into the control law. Finally, the performance for the proposed controller has been illustrated using the experimental results on a deployable suspended cable-driven robot showing the effectiveness of the proposed methodology regardless of the underlying system uncertainties.

Keywords Uncertain Jacobian · Cable-driven parallel manipulator · Passivity based control · Sliding mode control · Output redefinition

1 Introduction

A cable-driven parallel manipulator (CDPM) is a robot whose end-effector is controlled by winding and unwinding independent cables connecting it to the fixed base [1–3]. There are several advantages for these robots, including large workspace, high agility, and simple

✉ H.D. Taghirad
taghirad@kntu.ac.ir

1 Advanced Robotics and Automated Systems (ARAS), Industrial Control Center of Excellence (ICCE), Faculty of Electrical and Computer Engineering, K.N. Toosi University of Technology, Tehran, Iran

2 Department of Mechanical Engineering, Robotics Laboratory, Laval University, Quebec City, QC G1V 0A6, Canada

Published online: 20 November 2020

mechanical structures. Quick and easy deployment of cable-driven parallel robots was first proposed in [4–6]. Owing to their advantages, these classes of robots are suitable for many real-world applications, such as rescue missions [7] and automated farming [4].

The exact kinematic parameters for deployable suspended cable-driven robots (DSCRs) are generally unavailable. These inaccuracies induce many challenges in the process of designing a controller with suitable performance [8–10]. Despite these inaccuracies, these robots are suitable choices for many applications, where excellent precision is not required [11]. One example of such applications is sports field imaging. Developed by the ARAS research group, ARAS-CAM is a deployable DSCR designed explicitly for imaging applications.

Even though cables in CDPMs are often light-weight and follow flexible springs models [12–15], there are many real-world applications where cable dynamic analysis is of paramount importance [16–18]. For instance, in large-scale CDPMs with significant cable length variations, the simple spring model is not sufficient to represent the true dynamics. In these cases, understanding the cable dynamics is a key factor in understanding the specific aspects of the robot behavior [19]. An elastic cable leads to vibrations, deterioration of tracking accuracy, and in some cases, even loss of controllability [20]. Therefore, despite being challenging, dynamic models of cables has received a considerable amount of attention in the literature [21]. In [22], authors assume an axial spring model for the cables. However, this model is sufficiently accurate only for small-scale robots. In the case of large-scale manipulators, the cable dynamics causes delayed actuation at the end-effector. The distance between the actuator and the end-effector causes the system to become non-collocated, which limits the efficiency of conventional feedback controllers. In [23–26], this phenomenon has been modeled using the lumped mass method. This method concentrates the mass of the cable into a set of discrete lumped masses distributed along its length. The dynamics of the cable are modeled using spring and dampers between each discrete nodes. While the effect of gravity is not considered, Refs. [23, 24] have modeled the cable using lumped mass method. But in large cable robots, the effect of gravity is not negligible. Furthermore, in this research, no experimental results have been reported to show the performance of this method in a real application.

As stated earlier, this paper pursues two goals. The first goal is to propose a new control method suitable for deployable robots, while the second is to develop an algorithm that addresses the specific phenomenon caused by cable dynamics. These two goals are conflicting, and simultaneous achievement of them is very challenging. Indeed, in deployable cable-driven robots, use of expensive instruments shall be avoided, and sophisticated calibration procedures are not attainable. These limitations lead to high levels of model uncertainty. This uncertainty exacerbates the situation for the case of large-scale robots. Since, in this case, the model is more complicated, and the impact of uncertainty is more profound. This paper aims to present a novel control algorithm that utilizes inexpensive sensors to achieve suitable tracking accuracy and attenuated oscillations.

In the ARAS-CAM, a stereo camera is used to extract the end-effector position. Previously, the limited measurement rate of the visual feedback was addressed by integrating it with the encoder data [15, 27–29]. However, in these works, the overall stability of the system was not investigated. In this paper, a new control method is proposed with an integrated data fusion module, and its stability is investigated in details. Moreover, detailed examination of the robot's behavior is presented in this paper.

Furthermore, a more comprehensive model is developed with the purpose of proposing a proper controller to cope with cable vibrations. It is a known fact that in model-based control approaches, more complex models lead to overly complicated controllers that are not

applicable in practice. The purpose of this paper is to solve the problem while considering its practical implementation issues. To achieve this, we first present a complex and complete model for the robot using the lumped mass approach. Then, in order to decouple these complex equations, we assume that the payload is much heavier compared to the cables. This presumption allows us to assumed the dynamics to be decoupled and has been frequently used for controlling flexible robots in the literature [30–33]. Afterwards, based on the decoupled dynamic model, we proposed a light-weight and simple control law. This control method redefines a convex combination of the actuator speeds and the end-effector's velocity as output. The determination of this new output has no computational cost and applying the controller based on it reduces the undesirable vibrations of the end-effector. Due to this approximation, the robot's accuracy degrades but the undesired vibrations will significantly attenuate and smooth motions will be achieved.

The remainder of this paper is organized as follows. First, we present a brief introduction to the non-collocation property and passivity based control theory. In the next step, we introduce the ARAS-CAM robot and present its kinematic equations and Jacobian matrix. Next, we formulate the cable dynamics using the lumped mass model and present the overall dynamics of the ARAS-CAM cable-driven robot. In the next step, we introduce the proposed control law and analyze its stability and robustness. Finally, we present the experimental results and demonstrate that the proposed controller can achieve a suitable level of performance.

2 Underlying methods and theories

2.1 Non-collocation property in flexible systems

A robot is a collocated system if its sensors and their related actuators are located close to each other. In some mechanical systems, though such a configuration is not achievable because of practical limitations. In such cases, the robot is non-collocated, and sensors measure the feedback signals from locations other than the actuated points. Extensive researches have investigated these types of systems and have shown that small changes in the sensors location may lead to significant variations in the overall performance of the closed-loop system [34, 35]. For example, in the case of a linear system, the sensors location influences the number and placement of the system zeros and poles [36]. Flexible robots are one particular category of non-collocated systems where the dynamics of the flexible links separate the actuators and sensors. Generally speaking, poles of a system correspond to its natural frequencies and material properties, while zeros correspond to the relative position of sensors and actuators. In fact, in a flexible mechanism, the zeros model the flow of energy as it propagates throughout the system [36].

In the case of cable-driven robots with elastic cables, the non-collocation property of the system prevents a passive map between the actuators forces and the end-effector velocity. Therefore, it is impossible to use passivity based control (PBC) strategies for this family of robots.

Many researchers have addressed this problem by proposing the concept of redefined inputs and outputs [30–32]. It is showed that a passive relationship between theses newly defined ports could be achieved through this method [33, 37, 38]. These references define a μ parameter to scale the effect of the elastic coordinate system. In [23, 24], authors used this method to control a system with a single and two degrees of freedom motion. In what follows, we first present a brief introduction to passive mappings and their applications in the control theory. Then we use this method to control a DSCR.

2.2 An introduction to passivity

Consider the following system:

$$\begin{aligned} \dot{\boldsymbol{x}} &= \boldsymbol{f}(\boldsymbol{x}, \boldsymbol{u}), \\ \boldsymbol{y} &= \boldsymbol{h}(\boldsymbol{x}, \boldsymbol{u}), \end{aligned} \tag{1}$$

where $\boldsymbol{u}$ is the input vector, $\boldsymbol{y}$ is the output, and $\boldsymbol{x}$ is the system state variables. If one can find a positive definite functional V, such that

$$\dot{V} = \frac{\partial V}{\partial \boldsymbol{x}} \boldsymbol{f}(\boldsymbol{x}, \boldsymbol{u}) \leq \boldsymbol{u}^T \boldsymbol{y}, \tag{2}$$

the system is passive [39]. The physical interpretation for this is that the dissipation of energy in the overall system is larger than the stored energy. In other words,

$$V(\boldsymbol{x}(T)) - V(\boldsymbol{x}(0)) \leq \int_0^T \boldsymbol{y}^T(t)\boldsymbol{u}(t)dt. \tag{3}$$

The passivity theory states that a passive system controlled under negative feedback is stable in terms of L_2 criterion [39]. However, the main challenge is to prove the existence of passive dynamics relating the inputs and outputs. As such, here in this paper, we investigate the dynamical modeling of the robot considering the cable's mass and elasticity. Then we will show that the selection of appropriate inputs and outputs leads to a passive dynamic between them. After proving the existence of such dynamics, we employ the passivity theory and show that the system stability holds under a conventional feedback controller.

Even though we derive a comprehensive dynamic model for the robot, we do not directly use it for designing the controller. A controller synthesized using this model would be too complicated and not implementable. Moreover, depending on how inaccurate the model is, the deterioration of its response quality leads to a poor performance. Here, we aim to provide a practical solution for our problem by performing comprehensive modeling of the robot and showing that its stability can be maintained using well-known and easy to use PD controllers.

3 Introduction to ARAS-CAM

Developed in the ARAS robotics research group, ARAS-CAM robot, illustrated in Fig. 1, is a deployable suspended cable-driven manipulator with three degrees of translational freedom. This robot is a suitable tool for video capturing over a sport field or in the movie industry since it provides a large workspace, and it is easy to install. The robot end-effector is constrained to the ground through four cables, and therefore, it is categorized into redundantly actuated manipulators. The redundancy brings the robot several advantages. Firstly, the robot can cover a larger workspace since it has a better force distribution due to the redundancy [1]. Secondly, actuator redundancy leads to higher reliability, since even if we lose one cable, the robot can still operate safely. Thirdly, redundant robots can create larger forces, which leads to better agility. The robot requires no complex installation procedures and expensive pieces of equipment. As such, the ARAS-CAM belongs to the family of deployable and low-cost cable-driven robots.

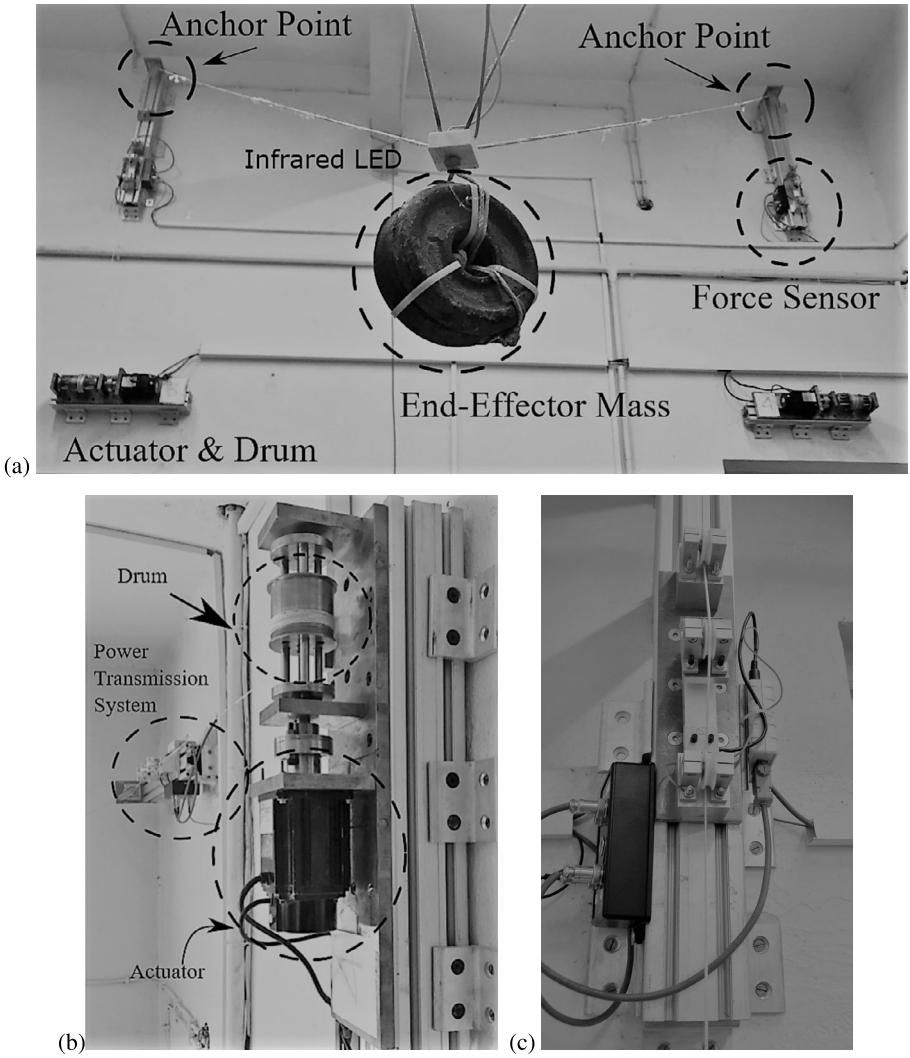

Fig. 1 (**a**) Prototype of a deployable suspended cable driven robot called ARAS-CAM, (**b**) the winch system, (**c**) the force sensor

3.1 ARAS-CAM structure

There are three types of sensors installed on the ARAS-CAM. In this section, we briefly introduce them.

3.1.1 Cable length measurement system

Each actuator in the robot controls a drum whose rotation determines the cable lengths. On the other hand, an incremental encoder measures the angular displacement of the motor shaft. Since this angular motion is linearly related to the cable length variation, the encoders

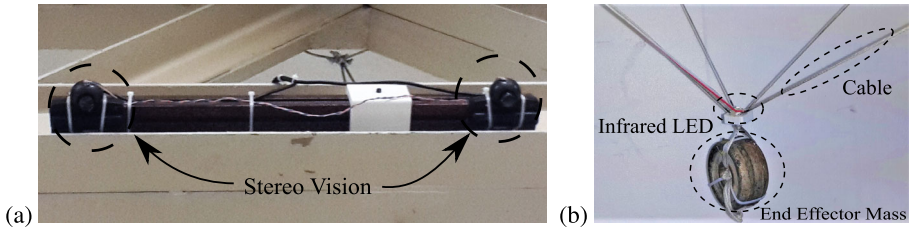

Fig. 2 (**a**) The prototype of a stereo vision system, (**b**) the LED attached to end-effector

can accurately measure these variations and given an initial bias, the absolute length. These initial biases are among the parameters estimated during the startup calibration process.

3.1.2 Force sensors

A single-axis load cell on each actuator unit measures the cable tension. As a cable leaves the drum, it passes through a pulley mechanism whose aim is to redirect the cable tension along the sensitive axis of the load cell. This mechanism is illustrated in Fig. 1. In the previous versions of the robot, the load cells were installed in between the cables and the end-effector. Even though this is a simple solution, it has two main drawbacks. First, the signal wires of the load cells hang over the end-effector and undermine its usefulness in real-world scenarios. Second, the load-cell's weight reduces the model accuracy, since it assumes straight cables, which is violated by the load-cell weight.

3.1.3 Vision based IR tracker

We measure the 3D position of the end-effector using a simple and inexpensive IR tracker system. This system tracks the 3D position of an IR LED attached to the robot's moving platform. Figure 2(b) illustrates the infrared LED attached to the robot end-effector, and Fig. 2(a) shows the designed stereo vision system. The camera system is developed using two PS3-EYE cameras with modified lenses. In front of each camera, a visible light filter blocks all the ambient light and allows only the LED's IR beam to pass through. Hence, the image captured by the camera is a shining white dot on a black screen. The two images form this stereo setup are then processed to retrieve the 3D location of the LED. This tracking system is capable of providing measurements at a rate of 60 Hz with an accuracy of 5 mm.

3.1.4 The real-time controller framework

The controller has been implemented using Matlab Simulink Real-Time Target(SLRT), which is a specialized real-time operating system created by Mathworks. The models are first designed in the Matlab software and then deployed to an independent PC running SLRT kernel. The model developed in Matlab contains some specific blocks that receive measurements from the robot and set the analog output channels of the DAQ cards to command the servo drives. In our specific setup, we receive the measurements through UDP and send the control commands using Advantech Analog DAQ cards.

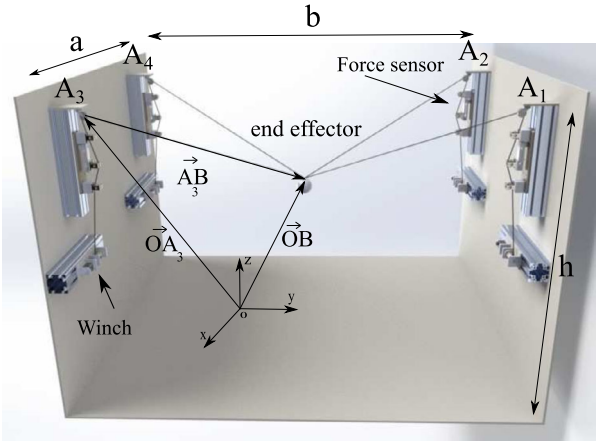

Fig. 3 The structure of a deployable suspended cable-driven robot

3.2 ARAS-CAM kinematics formulation

In this section, we derive the kinematic models for the ARAS-CAM robot. First, we present the forward and inverse kinematic equations, and next, through differentiation, we will derive the Jacobian matrix. Figure 3 depicts the schematic of the robot. As illustrated in this figure, four cables constrain the robot end-effector to the four fixed anchor locations on the base. In this paper, the equations are derived considering a lumped mass model for the end-effector. Based on Fig. 3, the loop closure equations can be written as follows:

$$\overrightarrow{A_jB} = \overrightarrow{OB} - \overrightarrow{OA_j}, \quad j = 1, \ldots, 4. \tag{4}$$

Let us define vector $\boldsymbol{l}_j = \overrightarrow{A_jB} = (l_{x_j}, l_{y_j}, l_{z_j})^T$ as the cable length variable. Moreover, define vectors $\boldsymbol{x} = \overrightarrow{OB} = (x, y, z)^T$ and $\boldsymbol{p}_j = \overrightarrow{OA_j} = (p_{x_j}, p_{y_j}, p_{z_j})^T$ as the end-effector position and the jth anchor point location, respectively. In what follows, the inverse kinematics and the Jacobian equations of the robot are derived.

3.2.1 Inverse kinematics

The algebraic loop closure equations representing the robot kinematics may be written as follows:

$$l_j^2 = (\boldsymbol{x} - \boldsymbol{p}_j)^T(\boldsymbol{x} - \boldsymbol{p}_j), \tag{5}$$

in which l_j represents the jth cable length. This equation can be decomposed as follows:

$$l_j = \sqrt{(x - p_{x_j})^2 + (y - p_{y_j})^2 + (z - p_{z_j})^2}, \tag{6}$$

where x, y, z and $p_{x_j}, p_{y_j}, p_{z_j}$, respectively, represent the components of end-effector's position and jth anchor point location.

3.2.2 Forward kinematics

To solve for the end-effector's position given the cable lengths, only three out of four equations presented in Eq. (6) suffice. For instance, given the cable lengths l_j, $j = 1, 2, 3$, the

position may be solved for as follows:

$$\begin{aligned} x &= \frac{1}{2a}(l_2^2 - l_1^2), \quad y = \frac{1}{2b}(l_3^2 - l_1^2), \\ z &= h \pm \sqrt{l_1^2 - (x + \frac{a}{2})^2 - (y + \frac{b}{2})^2}, \end{aligned} \tag{7}$$

where a, b and h can be easily found from the geometry shown in Fig. 3. There are two solutions for the z component. Based on the structure of the robot and the chosen coordinate systems, the only plausible solution is the negative one.

3.2.3 Jacobian matrix

The Jacobian matrix provides a map between task-space force and velocity and their joint-space counterparts, $\dot{\boldsymbol{l}}_c$, and cable tensions [1]. Furthermore, the singular values of this matrix provide a means for analyzing the workspace of the robot, which is of paramount importance for path planning and structural optimization tasks. The Jacobian for our robot is derived as follows. Given the vector of cable lengths $\boldsymbol{l}_c = (l_1, \ldots, l_4)$ and end-effector position $\boldsymbol{x} = (x, y, z)$, the kinematic equations may be arranged into the $\boldsymbol{f}(\boldsymbol{l}_c, \boldsymbol{x}) = 0$ implicit form. Using this function, the relation between $\dot{\boldsymbol{l}}_c$ and $\dot{\boldsymbol{x}}$ may be derived through differentiation as follows:

$$\boldsymbol{J}_x \dot{\boldsymbol{x}} = \boldsymbol{J}_l \dot{\boldsymbol{l}}_c, \tag{8}$$

$$\boldsymbol{J}_x = +\frac{\partial \boldsymbol{f}}{\partial \boldsymbol{x}}, \qquad \boldsymbol{J}_l = -\frac{\partial \boldsymbol{f}}{\partial \boldsymbol{l}_c}. \tag{9}$$

This yields the Jacobian matrix:

$$\dot{\boldsymbol{l}}_c = \boldsymbol{J} \dot{\boldsymbol{x}}, \tag{10}$$

$$\boldsymbol{J} = \boldsymbol{J}_L^{-1} \boldsymbol{J}_x. \tag{11}$$

For our robot, this matrix is as follows:

$$\boldsymbol{J} = \begin{bmatrix} \frac{(x-p_{x_1})}{l_1} & \frac{(y-p_{y_1})}{l_1} & \frac{(z-p_{z_1})}{l_1} \\ \frac{(x-p_{x_2})}{l_2} & \frac{(y-p_{y_2})}{l_2} & \frac{(z-p_{z_2})}{l_2} \\ \frac{(x-p_{x_3})}{l_3} & \frac{(y-p_{y_3})}{l_3} & \frac{(z-p_{z_3})}{l_3} \\ \frac{(x-p_{x_4})}{l_4} & \frac{(y-p_{y_4})}{l_4} & \frac{(z-p_{z_4})}{l_4} \end{bmatrix}. \tag{12}$$

4 Dynamics formulation

In this section, each cable is modeled in the form of discrete masses connected by springs and dampers. The dynamic model of one cable combined with the dynamics of its corresponding actuator forms that of a robot branch. The final dynamic model of the robot is formed by integrating the dynamic models of the four kinematic branches. The model considered in this section is written under the assumption of the dominant dynamics of longitudinal vibration, i.e., it is assumed that the sagging effect and the lateral vibration of cables are negligible.

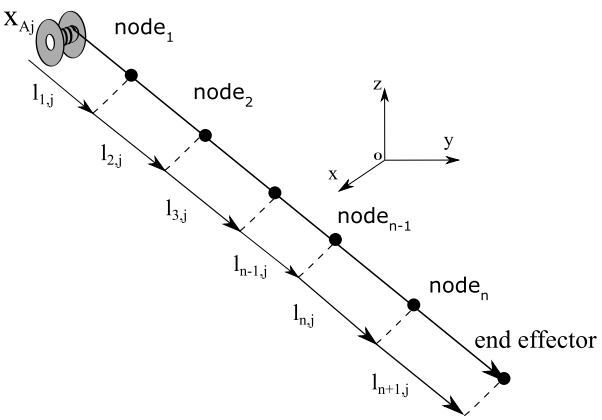

Fig. 4 Discrete mass modeling of cable

Regardless of the flexibility and cable mass, the robot's dynamics equations may be rewritten in general form can be as follows:

$$\boldsymbol{M}\ddot{\boldsymbol{x}} + \boldsymbol{C}\dot{\boldsymbol{x}} + \boldsymbol{g} = -\boldsymbol{J}^T\boldsymbol{\tau}, \tag{13}$$

in which $\boldsymbol{M}$, $\boldsymbol{C}$ and $\boldsymbol{g}$ denote the mass matrix, the Coriolis and centripetal matrix, and the gravity vector, respectively. It should be noted that in ARAS-CAM the end-effector has been considered as a point mass, thus, its Coriolis and centripetal matrices are zero. However, for the sake of generality, the dynamic equation are written in a generic form usable for most robots. In addition, $\boldsymbol{\tau}$ denote the vectors of the cable forces applied to the end-effector and $\boldsymbol{J}$ denotes the Jacobian matrix of the robot. This model defines the structural dynamics of the robot. In the following, we model each cable as a series of point masses connected by massless linear springs, such that the cable length added or reduced by the actuator only affects the length of the first section. It should be noted that considering such a model for cable is only valid under the assumption that the workspace is limited. With this assumption, the number of discrete masses considered for each cable is constant and does not change during the robot maneuvers. Therefore, the model considered for the robot is time-invariant. Moreover, as mentioned in [17], the dominant dynamic for the cables in a cable driven robot are due to axial vibrations. According to this fact, the cables can be modeled as a linear chain of spring-mass elements. Such a model is shown in Fig. 4. The position of masses in each section of the cable is defined by $l_{i,j}$, where i stands for the lumped-mass index, and j is the number of cables. The following equations denote the $l_{i,j}$:

$$\begin{aligned}
&l_{1,j} = l_{0_j}/(n+1) + r\theta_j + x_{g_{1j}} + x_{1,j},\\
&l_{2,j} = l_{0_j}/(n+1) + x_{g_{2,j}} + x_{2,j},\\
&\vdots\\
&l_{i,j} = l_{0_j}/(n+1) + x_{g_{i,j}} + x_{i,j},\\
&\vdots\\
&l_{n+1,j} = l_{0_j}/(n+1) + x_{g_{n+1,j}} + x_{n+1,j},
\end{aligned} \tag{14}$$

where $x_{i,j}$ states the relative flexible coordinates of ith section of the jth cable. The variable n represents the number of lumped mass for each cable. $x_{g_{i,j}}$ indicates the stretched length caused by the robot's weight. The parameter r also represents the radius of the drum and l_{0_j} indicates the initial length of jth cable. Variable θ_j shows the angle of the jth actuator. According to the above equations, the position of the lumped mass center may be derived as follows:

$$\begin{aligned}
&v_{1,j} = l_{1,j},\\
&v_{2,j} = l_{1,j} + l_{2,j},\\
&\vdots\\
&v_{i,j} = l_{1,j} + l_{2,j} + \cdots + l_{i,j},\\
&\vdots\\
&v_{n+1,j} = l_{1,j} + l_{2,j} + \cdots + l_{n+1,j}.
\end{aligned} \tag{15}$$

The stress of each part of the cable is also calculated as $\tau_{i,j} = k(x_{i,j} + x_{g_{i,j}}) + d\dot{x}_{i,j}$ where k represents the cable stiffness and d is the cable damping coefficient. It is important to note that in this paper, we assume that the mechanical homogeneous over the cable lengths, so that the same values of k and d are used for all cable segments. Moreover, $\boldsymbol{\tau} = [\tau_{n+1,1}, \tau_{n+1,2}, \tau_{n+1,3}, \tau_{n+1,4}]$ is the vector force of the end-effector applied by the end section of the cables. Therefore, the dynamic equations of each cable can be expressed as follows:

$$\begin{aligned}
&I_{m_j}\ddot{\theta}_j - r\tau_{1,j} = u_j,\\
&m_{1,j}\ddot{v}_{1,j} + \tau_{1,j} - m_{1,j}\frac{m_{1,j}}{l_j}\boldsymbol{l}_j^T\bar{\boldsymbol{g}} = \tau_{2,j},\\
&m_{2,j}\ddot{v}_{2,j} + \tau_2 - \frac{m_{2,j}}{l_j}\boldsymbol{l}_j^T\bar{\boldsymbol{g}} = \tau_{3,j},\\
&\vdots\\
&m_{n,j}\ddot{v}_n + \tau_{n,j} - \frac{m_{n,j}}{l_j}\boldsymbol{l}_j^T\bar{\boldsymbol{g}} = \tau_{n+1,j}.
\end{aligned} \tag{16}$$

In the above equations, I_{m_j} and r are the inertia matrix and the radius of the actuator system, respectively. Furthermore, $m_{i,j}$ stands for the mass of ith section in jth cable. Moreover, $\boldsymbol{l}_j$ is as defined in Eq. (4) and $l_j = \|\boldsymbol{l}_j\|$ indicates the overall length of the jth cable. It should be noted that $\frac{\boldsymbol{l}_j^T}{\|\boldsymbol{l}_j\|}$ represents the direction of the jth cable. Finally, the vector $\bar{\boldsymbol{g}}$ represents the Earth's gravity vector. To simplify and eliminate the gravity term from the above equations, static equations may be investigated. In the static case, the accelerations are all zero, and the amount of tension in the cable is solely determined by the mass of the end-effector and cables. Therefore, we have

$$\begin{aligned}
&kx_{g_{1,j}} = kx_{g_{2,j}} + \frac{m_{1,j}}{l_j}\boldsymbol{l}_j^T\bar{\boldsymbol{g}},\\
&kx_{g_{2,j}} = kx_{g_{3,j}} + \frac{m_{2,j}}{l_j}\boldsymbol{l}_j^T\bar{\boldsymbol{g}},\\
&\vdots\\
&kx_{g_{n,j}} = kx_{g_{n+1,j}} + \frac{m_{n,j}}{l_j}\boldsymbol{l}_j^T\bar{\boldsymbol{g}}.
\end{aligned} \tag{17}$$

Considering the above equations and $\tau_{i,j} = k(x_{i,j} + x_{g_{i,j}}) + d\dot{x}_{i,j}$, Eq. (16) can be rewritten as

$$\begin{aligned}
&I_{m_j}\ddot{\theta}_j - r\tau_{1,j} = u_j,\\
&m_{1,j}\ddot{v}_{1,j} + kx_{1,j} + d\dot{x}_{1,j} = kx_{2,j} + d\dot{x}_{2,j},\\
&m_{2,j}\ddot{v}_{2,j} + kx_{2,j} + d\dot{x}_{2,j} = kx_{3,j} + d\dot{x}_{3,j},\\
&\vdots\\
&m_n\ddot{v}_n + kx_{n,j} + d\dot{x}_{n,j} = kx_{n+1,j} + d\dot{x}_{n+1,j}.
\end{aligned} \tag{18}$$

By replacing the equivalent of $v_{i,j}$ in the above equations and by differentiation from Eq. (14), we can find the equivalent of $\ddot{l}_{1,j}$:

$$\begin{aligned}
&I_{m_j}\ddot{\theta}_j - r\tau_{1,j} = u_j,\\
&m_{1,j}(r\ddot{\theta}_j + \ddot{x}_{1,j}) + kx_{1,j} + d\dot{x}_{1,j} = kx_{2,j} + d\dot{x}_{2,j},\\
&m_{2,j}(r\ddot{\theta}_j + \ddot{x}_{1,j} + \ddot{x}_{2,j}) + kx_{2,j} + d\dot{x}_{2,j} = kx_{3,j} + d\dot{x}_{3,j},\\
&\vdots\\
&m_{n,j}(r\ddot{\theta}_j + \ddot{x}_{1,j} + \ddot{x}_{2,j} + \cdots + \ddot{x}_{n,j}) + kx_{n,j} + d\dot{x}_{n,j} = kx_{n+1,j} + d\dot{x}_{n+1,j}.
\end{aligned} \tag{19}$$

Then the above equations are rewritten in the matrix form:

$$\begin{bmatrix}
I_{m_j} & 0 & 0 & \dots & 0\\
rm_{1,j} & m_{1,j} & 0 & \dots & 0\\
rm_{2,j} & m_{2,j} & m_{2,j} & \dots & 0\\
\vdots & \vdots & \vdots & \vdots & \vdots\\
rm_{n,j} & m_{n,j} & m_{n,j} & \dots & m_{n,j}
\end{bmatrix}
\begin{bmatrix}
\ddot{\theta}_j\\ \ddot{x}_{1,j}\\ \ddot{x}_{2,j}\\ \vdots\\ \ddot{x}_{n,j}
\end{bmatrix} +
\begin{bmatrix}
-r\tau_{1,j}\\
k(x_{1,j} - x_{2,j}) + d(\dot{x}_{1,j} - \dot{x}_{2,j})\\
k(x_{2,j} - x_{3,j}) + d(\dot{x}_{2,j} - \dot{x}_{3,j})\\
\vdots\\
k(x_{n,j} - x_{n+1,j}) + d(\dot{x}_{n,j} - \dot{x}_{n+1,j})
\end{bmatrix} =
\begin{bmatrix}
u_j\\ 0\\ 0\\ \vdots\\ 0
\end{bmatrix}. \tag{20}$$

Equation (20) may be rewritten as the following equation in which the effect of $\boldsymbol{u}$ is visible in all rows:

$$\begin{bmatrix}
I_{m_j} & 0 & 0 & \dots & 0\\
r^{-1}I_{m_j} + rm_{1,j} & m_{1,j} & 0 & \dots & 0\\
r^{-1}I_{m_j} + rm_{1,j} + rm_{2,j} & m_{1,j} + m_{2,j} & m_{2,j} & \dots & 0\\
\vdots & \vdots & \vdots & \vdots & \vdots\\
r^{-1}I_{m_j} + rm_{1,j} + \cdots + rm_{n,j} & m_{1,j} + \cdots m_{n,j} & m_{2,j} + m_{n,j} & \dots & m_{n,j}
\end{bmatrix}
\begin{bmatrix}
\ddot{\theta}_j\\ \ddot{x}_{1,j}\\ \ddot{x}_{2,j}\\ \vdots\\ \ddot{x}_{n,j}
\end{bmatrix}$$

$$+\begin{bmatrix} -rkx_{1,j} - rd\dot{x}_{1,j} - rkx_{g_{1,j}} \\ -kx_{2,j} - d\dot{x}_{2,j} - r^{-1}kx_{g_{1,j}} \\ -kx_{3,j} - d\dot{x}_{3,j} - r^{-1}kx_{g_{1,j}} \\ \vdots \\ -kx_{n+1,j} - d\dot{x}_{n+1,j} - r^{-1}kx_{g_{1,j}} \end{bmatrix} = \begin{bmatrix} u_j \\ r^{-1}u_j \\ r^{-1}u_j \\ \vdots \\ r^{-1}u_j \end{bmatrix}. \tag{21}$$

Here we have multiplied the first row by r^{-1} and added the result to the second row and replaced the second row with the result. Then we add up the second and third rows and place the result in the new third row. We repeat this process until the last row, generating a new equation at each iteration. To simplify, we rewrite the above equations as

$$\boldsymbol{M}_{c_j}\begin{bmatrix} \ddot{\theta}_j \\ \ddot{\boldsymbol{x}}_{e_j} \end{bmatrix} - \boldsymbol{\tau}_{c_j} = \boldsymbol{u}_{c_j}, \tag{22}$$

in which

$$\boldsymbol{M}_{c_j} = \begin{bmatrix} I_{m_j} & 0 & 0 & \dots & 0 \\ r^{-1}I_{m_j} + rm_{1,j} & m_{1,j} & 0 & \dots & 0 \\ r^{-1}I_{m_j} + rm_{1,j} + rm_{2,j} & m_{1,j} + m_{2,j} & m_{2,j} & \dots & 0 \\ \vdots & \vdots & \vdots & \vdots & \vdots \\ r^{-1}I_{m_j} + rm_{1,j} + \dots + rm_{n,j} & m_{1,j} + \dots + m_{n,j} & m_{2,j} + m_{n,j} & \dots & m_{n,j} \end{bmatrix},$$

$$\boldsymbol{x}_{e_j} = \begin{bmatrix} x_{1,j} \\ x_{2,j} \\ \vdots \\ x_{n,j} \end{bmatrix}, \qquad \boldsymbol{\tau}_{c_j} = \begin{bmatrix} rkx_{1,j} + rd\dot{x}_{1,j} + rkx_{g_{1,j}} \\ kx_{2,j} + d\dot{x}_{2,j} + r^{-1}kx_{g_{1,j}} \\ kx_{3,j} + d\dot{x}_{3,j} + r^{-1}kx_{g_{1,j}} \\ \vdots \\ kx_{n+1,j} + d\dot{x}_{n+1,j} + r^{-1}kx_{g_{1,j}} \end{bmatrix},$$

$$\boldsymbol{u}_{c_j} = [u_j, r^{-1}u_j, r^{-1}u_j, \dots, r^{-1}u_j]^T. \tag{23}$$

We have such equations for all cables, therefore

$$\boldsymbol{M}_c\begin{bmatrix} \ddot{\theta}_1 \\ \ddot{\boldsymbol{x}}_{e_1} \\ \vdots \\ \ddot{\theta}_4 \\ \ddot{\boldsymbol{x}}_{e_4} \end{bmatrix} - \boldsymbol{\tau}_c = \boldsymbol{u}_c, \tag{24}$$

where

$$\boldsymbol{M}_c = diag(\boldsymbol{M}_{c_1}, \dots, \boldsymbol{M}_{c_4}), \qquad \boldsymbol{u}_c = [\boldsymbol{u}_{c_j}^T, \dots, \boldsymbol{u}_{c_4}^T]^T. \tag{25}$$

Finally, the two classes of equations can be integrated:

$$\boldsymbol{M}(\boldsymbol{x})\ddot{\boldsymbol{x}} + \boldsymbol{C}(\boldsymbol{x}, \dot{\boldsymbol{x}})\dot{\boldsymbol{x}} + \boldsymbol{g} = -\boldsymbol{J}^T\boldsymbol{\tau},$$

$$\boldsymbol{M}_c \begin{bmatrix} \ddot{\theta}_1 \\ \ddot{\boldsymbol{x}}_{e_1} \\ \vdots \\ \ddot{\theta}_4 \\ \ddot{\boldsymbol{x}}_{e_4} \end{bmatrix} - \boldsymbol{\tau}_c = \boldsymbol{u}_c. \tag{26}$$

4.1 Simplified dynamics formulation

In order to simplify the representation of the derived equations for the robot, we use the assumption expressed in [31]. In this reference, to decouple the equations involving rigid-body coordinates from involving flexible coordinates, it is assumed that the mass of the end-effector is much larger than those of the robot's links. Therefore, the overall kinetic energy of the system can be written as a result of the kinetic energy of two subsystems. The first subsystem is a robot in which the kinetic energy of the end-effector is dominant. The second subsystem is a robot links in which the kinetic energy of the flexible system is dominant. These assumptions are valid when the mass of the end-effector is much larger than that of the robot cables, which is the case for the first subsystem. Hence, when the end-effector is quiescent, the kinetic energy of the robot is mainly due to the speed and acceleration of the flexible coordinate.

4.2 Extracting the non-elastic dynamics formulation

Based on the above mentioned assumption, the majority of the kinetic energy of the system is owned by the end-effector when it is in motion. In contrast, when the end-effector is at rest, the kinetic energy of the robot depends on the flexible subsystem. With this assumption, the robot equations can be drastically simplified. To this end, we first rewrite Eq. (20)

$$\begin{bmatrix} I_{m_j} & 0 & 0 & \dots & 0 \\ rm_{1,j} & m_{1,j} & 0 & \dots & 0 \\ rm_{2,j} & m_{2,j} & m_{2,j} & \dots & 0 \\ \vdots & \vdots & \vdots & \vdots & \vdots \\ rm_{n,j} & m_{n,j} & m_{n,j} & \dots & m_{n,j} \end{bmatrix} \begin{bmatrix} \ddot{\theta}_j \\ \ddot{x}_{1,j} \\ \ddot{x}_{2,j} \\ \vdots \\ \ddot{x}_{n,j} \end{bmatrix} + \begin{bmatrix} -r\tau_{1,j} \\ k(x_{1,j} - x_{2,j}) + d(\dot{x}_{1,j} - \dot{x}_{2,j}) \\ k(x_{2,j} - x_{3,j}) + d(\dot{x}_{2,j} - \dot{x}_{3,j}) \\ \vdots \\ k(x_{n,j} - x_{n+1,j}) + d(\dot{x}_{n,j} - \dot{x}_{n+1,j}) \end{bmatrix} = \begin{bmatrix} u_j \\ 0 \\ 0 \\ \vdots \\ 0 \end{bmatrix}. \tag{27}$$

Then we assume that the end-effector is moving and the kinetic energy of the system all are due to this mass. This is a proper approximation frequently used in the literature [23, 24, 30–33]. This approximation is based on the assumption that the mass of the end-effector is much larger than the mass of the cables, which allows for an approximate decoupling of the dynamics. Thus, assuming that $\ddot{\boldsymbol{x}}_{i,j}$ and $\ddot{\boldsymbol{x}}_{i,j}$ are zero, the above equations can be rewritten

as

$$\begin{aligned} &I_{m_j}\ddot{\theta}_j - r\tau_{1,j} = u_j, \\ &x_{1,j} - x_{2,j} = 0, \\ &x_{2,j} - x_{3,j} = 0, \\ &\vdots \\ &x_{n,j} - x_{n+1,j} = 0. \end{aligned} \tag{28}$$

By blending the $n+1$ equations stated in Eq. (28) in one equation, we have

$$I_{m_j}\ddot{\theta}_j - rk(x_{n+1,j} + x_{g_{1,j}}) = u_j. \tag{29}$$

On the other hand, according to Eq. (17), the static equations governing on $x_{g_{1,j}}$ are given by

$$kx_{g_{1,j}} = (m_{1,j} + m_{2,j} + \cdots + m_{n,j})\frac{\boldsymbol{l}_j^T}{l_j}\bar{\boldsymbol{g}} + kx_{g_{n+1,j}}. \tag{30}$$

According to the above equation and Eq. (29) and considering $\tau_{n+1,j} = kx_{n+1,j} + kx_{g_{n+1,j}}$, we have

$$I_{m_j}\ddot{\theta}_j - r\tau_{n+1,j} - r(m_{1,j} + m_{2,j} + \cdots + m_{n,j})\frac{\boldsymbol{l}_j^T}{l_j}\bar{\boldsymbol{g}} = u_j. \tag{31}$$

Then we rewrite the above equation in a matrix form for all cables as follows:

$$\boldsymbol{I}_c\ddot{\boldsymbol{\theta}} - r\boldsymbol{\tau} + \boldsymbol{g}_c = \boldsymbol{u}, \tag{32}$$

in which

$$\begin{aligned} &\boldsymbol{I}_c = diag(I_{m_1}, \ldots, I_{m_4}), \qquad \boldsymbol{\tau} = [\tau_{n+1,1}, \ldots, \tau_{n+1,4}]^T, \qquad \boldsymbol{u} = [u_1, \ldots, u_4]^T, \\ &\boldsymbol{g}_c = -rdiag(m_{1,1} + m_{2,1} + \cdots + m_{n,1}, \ldots, m_{1,4} + m_{2,4} + \cdots + m_{n,4})\boldsymbol{L}\bar{\boldsymbol{g}}, \\ &\boldsymbol{L} = [\frac{\boldsymbol{l}_1^T}{l_1}; \ldots; \frac{\boldsymbol{l}_4^T}{l_4}], \qquad \boldsymbol{\theta} = [\theta_1, \ldots, \theta_4]^T. \end{aligned} \tag{33}$$

The above equation alongside the structural dynamic equation forms the overall dynamics of the robot:

$$\begin{aligned} &\boldsymbol{M}(\boldsymbol{x})\ddot{\boldsymbol{x}} + \boldsymbol{C}(\boldsymbol{x}, \dot{\boldsymbol{x}})\dot{\boldsymbol{x}} + \boldsymbol{g} = -\boldsymbol{J}^T\boldsymbol{\tau} \\ &\boldsymbol{I}_c\ddot{\boldsymbol{\theta}} - r\boldsymbol{\tau} + \boldsymbol{g}_c = \boldsymbol{u}. \end{aligned} \tag{34}$$

Considering that $r\ddot{\boldsymbol{\theta}} = \boldsymbol{J}\ddot{\boldsymbol{x}} + \dot{\boldsymbol{J}}\dot{\boldsymbol{x}}$, we may simplify the above equation as follows:

$$\boldsymbol{M}_T\ddot{\boldsymbol{x}} + \boldsymbol{C}_T\dot{\boldsymbol{x}} + \boldsymbol{g}_T = \boldsymbol{J}^T\boldsymbol{u}, \tag{35}$$

where

$$\boldsymbol{M}_T = \boldsymbol{M} + r^{-1}\boldsymbol{J}^T\boldsymbol{I}_c\boldsymbol{J}, \qquad \boldsymbol{C}_T = \boldsymbol{C} + r^{-1}\boldsymbol{J}^T\boldsymbol{I}_c\dot{\boldsymbol{J}}, \qquad \boldsymbol{g}_T = \boldsymbol{g} + \boldsymbol{J}^T\boldsymbol{g}_c. \tag{36}$$

4.3 Extracting elastic dynamics formulation

On the contrary, if we assume that the end-effector is at rest and that the variables $\dot{\boldsymbol{x}}$ and $\ddot{\boldsymbol{x}}$ are zero, then Eq. (26) are converted into

$$\begin{aligned} \boldsymbol{g} &= -\boldsymbol{J}^T \boldsymbol{\tau}, \\ \boldsymbol{M}_c \ddot{\boldsymbol{q}} - \boldsymbol{\tau}_c &= \boldsymbol{u}_c. \end{aligned} \tag{37}$$

Regarding the relation between the elastic system variables mentioned in Eq. (15), we have

$$\ddot{v}_{n+1,j} = \ddot{l}_{1,j} + \ddot{l}_{2,j} + \cdots + \ddot{l}_{n,j} + \ddot{l}_{n+1,j} = 0. \tag{38}$$

Therefore,

$$r\ddot{\theta}_j + \ddot{x}_{1,j} + \ddot{x}_{2,j} + \cdots + \ddot{x}_{i,j} \ldots + \ddot{x}_{n,j} + \ddot{x}_{n+1,j} = 0. \tag{39}$$

According to the above equation, one can express the variable $\ddot{\theta}_j$ in terms of the elastic coordinates:

$$\ddot{\theta}_j = -r^{-1}(\ddot{x}_{1,j} + \ddot{x}_{2,j} + \cdots + \ddot{x}_{i,j} \ldots + \ddot{x}_{n,j} + \ddot{x}_{n+1,j}). \tag{40}$$

Therefore, Eq. (21) may be written as

$$\begin{bmatrix} r^{-1}I_{m_j} & r^{-1}I_{m_j} & r^{-1}I_{m_j} \\ r^{-2}I_{m_j} & r^{-2}I_{m_j} + m_{1,j} & r^{-2}I_{m_j} + m_{1,j} \\ r^{-2}I_{m_j} & r^{-2}I_{m_j} + m_{1,j} & r^{-2}I_{m_j} + m_{1,j} + m_{2,j} \\ r^{-2}I_{m_j} & r^{-2}I_{m_j} + m_{1,j} & r^{-2}I_{m_j} + m_{1,j} + m_{2,j} \\ \vdots & \vdots & \vdots \\ r^{-2}I_{m_j} & r^{-2}I_{m_j} + m_{1,j} & r^{-2}I_{m_j} + m_{1,j} + m_{2,j} \end{bmatrix}$$

$$\begin{bmatrix} \ldots & r^{-1}I_{m_j} \\ \ldots & r^{-2}I_{m_j} + m_{1,j} \\ \ldots & r^{-2}I_{m_j} + m_{1,j} + m_{2,j} \\ \ldots & r^{-2}I_{m_j} + m_{1,j} + m_{2,j} + m_{3,j} \\ \vdots & \vdots \\ \ldots & r^{-2}I_{m_j} + m_{1,j} + m_{2,j} + m_{3,j} + \cdots + m_{n,j} \end{bmatrix}$$

$$\times \begin{bmatrix} \ddot{x}_{1,j} \\ \ddot{x}_{2,j} \\ \vdots \\ \ddot{x}_{n,j} \\ \ddot{x}_{n+1,j} \end{bmatrix} + \begin{bmatrix} rkx_{1,j} + rd\dot{x}_{1,j} + rkx_{g_{1,j}} \\ rkx_{2,j} + rd\dot{x}_{2,j} + rkx_{g_{1,j}} \\ rkx_{3,j} + rd\dot{x}_{3,j} + rkx_{g_{1,j}} \\ \vdots \\ rkx_{n+1,j} + rd\dot{x}_{n+1,j} + rkx_{g_{1,j}} \end{bmatrix} = - \begin{bmatrix} u_j \\ u_j \\ u_j \\ \vdots \\ u_j \end{bmatrix}. \tag{41}$$

These equations can be rewritten as

$$\boldsymbol{M}_{e_j} \ddot{\boldsymbol{x}}_{e_j} + \boldsymbol{D}_{e_j} \dot{\boldsymbol{x}}_{e_j} + \boldsymbol{K}_{e_j} \boldsymbol{x}_{e_j} + \boldsymbol{g}_{e_j} = -\boldsymbol{u}_{e_j}, \tag{42}$$

in which

$$\boldsymbol{M}_{e_j} = \begin{bmatrix} r^{-1}I_{m_j} & r^{-1}I_{m_j} & r^{-1}I_{m_j} \\ r^{-2}I_{m_j} & r^{-2}I_{m_j}+m_{1,j} & r^{-2}I_{m_j}+m_{1,j} \\ r^{-2}I_{m_j} & r^{-2}I_{m_j}+m_{1,j} & r^{-2}I_{m_j}+m_{1,j}+m_{2,j} \\ r^{-2}I_{m_j} & r^{-1}I_{m_j}+m_{1,j} & r^{-2}I_{m_j}+m_{1,j}+m_{2,j} \\ \vdots & \vdots & \vdots \\ r^{-2}I_{m_j} & r^{-2}I_{m_j}+m_{1,j} & r^{-2}I_{m_j}+m_{1,j}+m_{2,j} \end{bmatrix}$$

$$\begin{bmatrix} \dots & r^{-1}I_{m_j} \\ \dots & r^{-2}I_{m_j}+m_{1,j} \\ \dots & r^{-2}I_{m_j}+m_{1,j}+m_{2,j} \\ \dots & r^{-1}I_{m_j}+m_{1,j}+m_{2,j}+m_{3,j} \\ \vdots & \vdots \\ \dots & r^{-2}I_{m_j}+m_{1,j}+m_{2,j}+m_{3,j}+\cdots+m_{n,j} \end{bmatrix}, \tag{43}$$

$$\boldsymbol{K}_{e_j} = \begin{bmatrix} rk & 0 & 0 & \dots & 0 & 0 \\ 0 & rk & 0 & \dots & 0 & 0 \\ 0 & 0 & rk & \dots & 0 & 0 \\ \vdots & & & & & \\ 0 & 0 & 0 & \dots & 0 & rk \end{bmatrix}, \qquad \boldsymbol{D}_{e_j} = \begin{bmatrix} rd & 0 & 0 & \dots & 0 & 0 \\ 0 & rd & 0 & \dots & 0 & 0 \\ 0 & 0 & rd & \dots & 0 & 0 \\ \vdots & & & & & \\ 0 & 0 & 0 & \dots & 0 & rd \end{bmatrix},$$

and

$$\begin{aligned} &\boldsymbol{x}_{e_j} = [x_{1,j}, x_{2,j}, \dots, x_{n,j}, x_{n+1,j}]^T, \qquad \boldsymbol{u}_{e_j} = [u_j, u_j, u_j, \dots, u_j]^T, \\ &\boldsymbol{g}_{e_j} = kx_{g_{1,j}}[1, \dots, 1]^T_{(n+1)\times 1}. \end{aligned} \tag{44}$$

Let us derive these equations for all four cables.

$$\boldsymbol{M}_e\ddot{\boldsymbol{x}}_e + \boldsymbol{D}_e\dot{\boldsymbol{x}}_e + \boldsymbol{K}_e\boldsymbol{x}_e + \boldsymbol{g}_e = -\boldsymbol{u}_e, \tag{45}$$

where

$$\begin{aligned} &\boldsymbol{M}_e = diag(\boldsymbol{M}_{e_1}, \dots, \boldsymbol{M}_{e_4}), \qquad \boldsymbol{D}_e = diag(\boldsymbol{D}_{e_1}, \dots, \boldsymbol{D}_{e_4}), \\ &\boldsymbol{K}_e = diag(\boldsymbol{K}_{e_1}, \dots, \boldsymbol{K}_{e_4}) \\ &\boldsymbol{u}_e = [\boldsymbol{u}_{e_1}, \dots, \boldsymbol{u}_{e_4}]^T \qquad \boldsymbol{x}_e = [\boldsymbol{x}_{e_1}, \dots, \boldsymbol{x}_{e_4}]^T, \qquad \boldsymbol{g}_e = [\boldsymbol{g}_{e_1}, \dots, \boldsymbol{g}_{e_4}]^T. \end{aligned} \tag{46}$$

Finally, considering Eqs. (35) and (45), we can state the dynamic equations of the non-elastic and elastic system as follows:

$$\begin{aligned} &\boldsymbol{M}_T\ddot{\boldsymbol{x}} + \boldsymbol{C}_T\dot{\boldsymbol{x}} + \boldsymbol{g}_T = \boldsymbol{f} \\ &\boldsymbol{M}_e\ddot{\boldsymbol{x}}_e + \boldsymbol{D}_e\dot{\boldsymbol{x}}_e + \boldsymbol{K}_e\boldsymbol{x}_e + \boldsymbol{g}_e = \boldsymbol{B}\boldsymbol{f}, \end{aligned} \tag{47}$$

in which

$$\boldsymbol{B} = -\Psi\,\boldsymbol{J}^{-T} \qquad \boldsymbol{f} = \boldsymbol{J}^T\boldsymbol{u}, \tag{48}$$

where

$$\Psi = \begin{bmatrix} \overrightarrow{1}_{n+1} & \overrightarrow{0}_{n+1} & \overrightarrow{0}_{n+1} & \overrightarrow{0}_{n+1} \\ \overrightarrow{0}_{n+1} & \overrightarrow{1}_{n+1} & \overrightarrow{0}_{n+1} & \overrightarrow{0}_{n+1} \\ \overrightarrow{0}_{n+1} & \overrightarrow{0}_{n+1} & \overrightarrow{1}_{n+1} & \overrightarrow{0}_{n+1} \\ \overrightarrow{0}_{n+1} & \overrightarrow{0}_{n+1} & \overrightarrow{0}_{n+1} & \overrightarrow{1}_{n+1} \end{bmatrix}_{(4n+4)\times 4}, \tag{49}$$

where $\overrightarrow{1}_{n+1} = [1, \ldots, 1]^T \in \mathbb{R}^{n+1}$ and $\overrightarrow{0}_{n+1} = [0, \ldots, 0]^T \in \mathbb{R}^{n+1}$. It can be shown that the vector $\boldsymbol{g}_e$ can be written as $\boldsymbol{g}_e = \boldsymbol{B}\boldsymbol{g}_T$.

4.4 Energy investigation of the two subsystem

The kinetic and potential energies of the non-elastic system can be stated as follows:

$$H_x = T_x + V_x, \tag{50}$$

in which T_x is

$$T_x = \frac{1}{2}\dot{\boldsymbol{x}}^T \boldsymbol{M}_T \dot{\boldsymbol{x}}. \tag{51}$$

The potential energy is also interpreted as follows:

$$\boldsymbol{g}_T = \frac{\partial V_x(\boldsymbol{x})}{\partial \boldsymbol{x}}. \tag{52}$$

On the other hand, the energy of the elastic system is $H_e = T_e + V_e$, in which T_e can be written as follows:

$$T_e = \frac{1}{2}\dot{\boldsymbol{x}}_e^T \boldsymbol{M}_e \dot{\boldsymbol{x}}_e, \tag{53}$$

and the potential energy V_e is

$$V_e = \frac{1}{2}\boldsymbol{x}_e^T \boldsymbol{K}_e \boldsymbol{x}_e + V_{ge}(\boldsymbol{x}_e), \tag{54}$$

where $V_{ge}(\boldsymbol{x}_e)$ represents the potential energy, which is associated with $\boldsymbol{x}_e$ as follows:

$$\boldsymbol{g}_e = \frac{\partial V_{ge}(\boldsymbol{x}_e)}{\partial \boldsymbol{x}_e}. \tag{55}$$

5 The proposed control law

As mentioned earlier, by using the PBC theory, the L_2 stability of a passive system, which is connected to a passive controller through negative feedback, is guaranteed [39]. Therefore, when passive mappings are detected between the input and outputs of a system, it is possible to ensure the stability of the system with well-known controllers such as PD.

As indicated in Refs. [31, 33, 40], in flexible systems, the relation between the actuator torque with the end-effector speed is not a passive mapping. This can be attributed to the non-collocation feature of these systems [33]. Several solutions have been proposed to remedy this problem, including the use of redefined output. By this means, and through the new output, alongside the input of the system, one can ensure the passivity of the map. Reference [33] calls this new output the μ tip rate.

5.1 μ tip rate

The velocity $\dot{\boldsymbol{x}}_\mu$ is defined as the μ convex combination of the speed of flexible coordinate and the end-effector by the following relation:

$$\dot{\boldsymbol{x}}_\mu = \dot{\boldsymbol{x}} + (1-\mu)\boldsymbol{B}^T\dot{\boldsymbol{x}}_e, \tag{56}$$

in which $\boldsymbol{x}$ and $\boldsymbol{x}_e$ denote the end-effector position and flexible coordinate, respectively. Furthermore, the matrix $\boldsymbol{B}$ is defined in Eq. (48). In the above equation, μ has a value between $[0, 1]$. The velocity $\dot{\boldsymbol{x}}_\mu$ can also be expressed as a combination of the speed of actuators and the end-effector. To this end, we add and subtract $\mu\dot{\boldsymbol{x}}$ to the Eq. (56):

$$\begin{aligned}\dot{\boldsymbol{x}}_\mu &= \dot{\boldsymbol{x}} + (1-\mu)\boldsymbol{B}^T\dot{\boldsymbol{x}}_e + \mu\dot{\boldsymbol{x}} - \mu\dot{\boldsymbol{x}} \\ &= \mu\dot{\boldsymbol{x}} + (1-\mu)(\dot{\boldsymbol{x}} + \boldsymbol{B}^T\dot{\boldsymbol{x}}_e).\end{aligned} \tag{57}$$

Considering Eq. (15) and according to relation velocity between end-effector motion and the other flexible coordinates, we have

$$\boldsymbol{J}\dot{\boldsymbol{x}} = r\dot{\boldsymbol{\theta}} + \Psi^T\dot{\boldsymbol{x}}_e, \tag{58}$$

in which $\boldsymbol{\theta}$ and r stand for the vector of actuator angles and the drum radius, respectively. Furthermore, the matrices $\boldsymbol{J}$ and Ψ are defined in Eqs. (11) and (49), respectively. According to the Eq. (58), the value of $r\boldsymbol{J}^{-1}\boldsymbol{\theta}$ can be written as follows:

$$r\boldsymbol{J}^{-1}\dot{\boldsymbol{\theta}} = \dot{\boldsymbol{x}} + \boldsymbol{B}^T\dot{\boldsymbol{x}}_e. \tag{59}$$

By substituting the above equation to Eq. (57), we have

$$\dot{\boldsymbol{x}}_\mu = \mu\dot{\boldsymbol{x}} + (1-\mu)r\boldsymbol{J}^{-1}\dot{\boldsymbol{\theta}}. \tag{60}$$

The above equation represents $\dot{\boldsymbol{x}}_\mu$ as a combination of the speed of actuators and the end-effector. The μ tip rate can be interpreted as the end-effector speed that is weighted using flexible coordinates. For example, when $\mu = 1$, the μ tip rate represents the exact end-effector speed, and the output only involves in the speed of actuators when $\mu = 0$. It should be noted that the μ tip rate may be extracted theoretically by merging the speeds of the end-effector and actuators with flexible coordinate. In practice, however, it might not be derived easily, since the speed of the flexible coordinate is difficult to measure. The physical concept of using the μ tip rate can be interpreted more straightforwardly. Suppose the robot is programmed to travel on a user-designed path The robot moves along this path with some oscillation, however. In order to suppress these oscillations by the control law, the difference between undesired vibrations shall be determined. The source of these oscillations cannot be determined if the only feedback is the position of the manipulator end-effector. In other words, oscillations caused by dynamic cables are not observable in this case. Therefore, it is necessary to provide feedback from the flexible coordinate of the robot. The most suitable alternative feedback on the robot that can provide information about the elastic coordinate system is the angular velocity of the actuators itself, measured by the encoders. Therefore, we wish to use both the end-effector position and information associated with the actuators to eliminate undesired oscillations and improve accuracy. Moreover, one may show that there is a passive connection between its input and output if the μ tip rate is selected as the redefined output of the cable driven robot.

Theorem 1 *Consider the cable robot system proposed in Eq. (47). For such a system, there is a passive map between the input and the output $\dot{\boldsymbol{x}}_\mu$ as defined in Eq. (56).*

Proof As the total energy of the system is $H = H_x + H_e$, we define H_μ as follows:

$$\begin{aligned} H_\mu &= H - \mu H_e \\ &= H_x + H_e - \mu H_e \\ &= H_x + (1-\mu) H_e; \end{aligned} \tag{61}$$

then we compute the derivative of the above equation to be

$$\begin{aligned} \dot{H}_\mu &= \dot{H}_x + (1-\mu)\dot{H}_e \\ &= \dot{T}_x + \dot{V}_x + (1-\mu)(\dot{T}_e + \dot{V}_e). \end{aligned} \tag{62}$$

Differentiate Eq. (51) and (54) and substitute in the above equation:

$$\dot{H}_\mu = \dot{\boldsymbol{x}}^T \boldsymbol{M}_T \ddot{\boldsymbol{x}} + \frac{1}{2}\dot{\boldsymbol{x}}^T \dot{\boldsymbol{M}}_T \dot{\boldsymbol{x}} + \dot{V}_x + (1-\mu)\dot{\boldsymbol{x}}_e^T \boldsymbol{M}_e \ddot{\boldsymbol{x}}_e + (1-\mu)\boldsymbol{x}_e^T \boldsymbol{K}_e \dot{\boldsymbol{x}}_e + (1-\mu)\dot{V}_{ge}. \tag{63}$$

Substitute the equivalent of the terms $\boldsymbol{M}_T \ddot{\boldsymbol{x}}$ and $\boldsymbol{M}_e \ddot{\boldsymbol{x}}_e$ from Eq. (47):

$$\begin{aligned} \dot{H}_\mu = {} & \dot{\boldsymbol{x}}^T(-\boldsymbol{C}_T \dot{\boldsymbol{x}} - \boldsymbol{g} + \boldsymbol{f}) + \frac{1}{2}\dot{\boldsymbol{x}}^T \dot{\boldsymbol{M}}_T \dot{\boldsymbol{x}} + \dot{V}_x + (1-\mu)\dot{\boldsymbol{x}}_e^T(\boldsymbol{B}\boldsymbol{f} - \boldsymbol{K}_e \boldsymbol{x}_e - \boldsymbol{D}_e \dot{\boldsymbol{x}}_e - \boldsymbol{g}_e) \\ & + (1-\mu)\boldsymbol{x}_e^T \boldsymbol{K}_e \dot{\boldsymbol{x}}_e + (1-\mu)\dot{V}_{ge}. \end{aligned} \tag{64}$$

Considering that $\dot{\boldsymbol{M}}_T - 2\boldsymbol{C}_T$ is skew-symmetric [1], according to Eqs. (52) and (55), the above equation may be written in the simpler form

$$\begin{aligned} \dot{H}_\mu &= \dot{\boldsymbol{x}}^T \boldsymbol{f} + (1-\mu)\dot{\boldsymbol{x}}_e^T \boldsymbol{B}\boldsymbol{f} - (1-\mu)\dot{\boldsymbol{x}}_e^T \boldsymbol{D}_e \dot{\boldsymbol{x}}_e \\ &= (\dot{\boldsymbol{x}}^T + (1-\mu)\dot{\boldsymbol{x}}_e^T \boldsymbol{B})\boldsymbol{f} - (1-\mu)\dot{\boldsymbol{x}}_e^T \boldsymbol{D}_e \dot{\boldsymbol{x}}_e. \end{aligned} \tag{65}$$

If we use Eq. (56), the above equation is simplified to

$$\dot{H}_\mu = \dot{\boldsymbol{x}}_\mu^T \boldsymbol{f} - (1-\mu)\dot{\boldsymbol{x}}_e^T \boldsymbol{D}_e \dot{\boldsymbol{x}}_e. \tag{66}$$

Integrating the above equation yields

$$\int_0^T \dot{\boldsymbol{x}}_\mu^T \boldsymbol{f}\, dt = H_\mu(T) - H_\mu(0) + (1-\mu)\int_0^T \dot{\boldsymbol{x}}_e^T \boldsymbol{D}_e \dot{\boldsymbol{x}}_e dt. \tag{67}$$

Therefore, when $0 \le \mu \le 1$, the system energy, i.e., $\int_0^T \dot{\boldsymbol{x}}_\mu^T \boldsymbol{f}\, dt$ will be greater than that stored $H_\mu(T) - H_\mu(0)$, which indicates that the mapping from $\boldsymbol{f}$ to $\dot{\boldsymbol{x}}_\mu$ is a passive mapping. It should be noted, when $\mu = 1$, that the above relation is on the boundary of passivity, such that the speed of the flexible coordinate is not observable. □

5.2 μ selection

Controller system design is often a trade-off between the achievable performance of the control system and the robustness of the controller against uncertainties. As it is clear from the definition of μ in Eq. (56), the redefined output is closer to the actual value of the end-effector speed, when μ is selected close to one. Such a large value for μ can lead to better system performance. In contrast, selecting a smaller value for μ may increase the robustness of the control system. It should be noted that the system would be passive for all values of μ greater than zero and smaller than one. However, as μ approaches one, the system reaches the passivity boundary. Therefore, a suitable choice for μ is set through a trade-off between system performance and robustness.

As mentioned in [33], when the mass ratio of the end-effector to cables is high, a large μ may be selected to favor performance. Conversely, when the ratio of end–effector mass to the cable masses is small, μ should be small to guarantee the robot stability. For example, by choosing $\mu = 0.9$, one can expect the system to remain passive and perform well, provided that the mass of the end-effector is at least five times the mass of the links and other inertia of the robot [33].

5.3 Robust passive controller

By using Eq. (56), a desired velocity can be defined as $\dot{\boldsymbol{x}}_{\mu,d} = \mu\dot{\boldsymbol{x}}_d + (1-\mu)r\boldsymbol{J}^{-1}\dot{\boldsymbol{\theta}}_d$. Let us consider a sliding surface as $\boldsymbol{s}_\mu = \dot{\tilde{\boldsymbol{x}}}_\mu + \Lambda\tilde{\boldsymbol{x}}_\mu$ in which Λ is a positive diagonal matrix and

$$\begin{aligned} \dot{\tilde{\boldsymbol{x}}}_\mu &= \dot{\boldsymbol{x}}_\mu - \dot{\boldsymbol{x}}_{\mu,d}, \\ \tilde{\boldsymbol{x}}_\mu &= \boldsymbol{x}_\mu - \boldsymbol{x}_{\mu,d}. \end{aligned} \tag{68}$$

A reference trajectory is also defined as

$$\dot{\boldsymbol{x}}_r = \dot{\boldsymbol{x}}_{\mu,d} - \Lambda\tilde{\boldsymbol{x}}_\mu. \tag{69}$$

The tracking error for $\dot{\boldsymbol{x}}_r$ is also defined as

$$\dot{\tilde{\boldsymbol{x}}}_r = \dot{\boldsymbol{x}} - \dot{\boldsymbol{x}}_r. \tag{70}$$

With some mathematical calculations, it can be shown that the sliding surface can be rewritten as

$$\begin{aligned} \boldsymbol{s}_\mu &= \dot{\tilde{\boldsymbol{x}}}_\mu + \Lambda\tilde{\boldsymbol{x}}_\mu \\ &= \dot{\boldsymbol{x}}_\mu - \dot{\boldsymbol{x}}_{\mu,d} + \Lambda\tilde{\boldsymbol{x}}_\mu. \end{aligned} \tag{71}$$

By adding and subtracting $\dot{\boldsymbol{x}}$ from the above equation, we have

$$\boldsymbol{s}_\mu = \dot{\boldsymbol{x}}_\mu - \dot{\boldsymbol{x}}_{\mu,d} + \Lambda\tilde{\boldsymbol{x}}_\mu - \dot{\boldsymbol{x}} + \dot{\boldsymbol{x}}. \tag{72}$$

According to Eq. (69), the above equation simplifies to

$$\boldsymbol{s}_\mu = \dot{\boldsymbol{x}}_\mu - \dot{\boldsymbol{x}}_r - \dot{\boldsymbol{x}} + \dot{\boldsymbol{x}}. \tag{73}$$

Through Eqs. (70) and (56), we have

$$\boldsymbol{s}_\mu = \dot{\tilde{\boldsymbol{x}}}_r + (1-\mu)\boldsymbol{B}^T\dot{\boldsymbol{x}}_e. \tag{74}$$

Using the Eq. (47) one can rewrite the dynamics equation of the reference trajectory as

$$\begin{aligned} \boldsymbol{M}_T\ddot{\boldsymbol{x}}_r + \boldsymbol{C}_T\dot{\boldsymbol{x}}_r + \boldsymbol{g}_T &= \boldsymbol{f}_r, \\ \boldsymbol{M}_e\ddot{\boldsymbol{x}}_{er} + \boldsymbol{D}_e\dot{\boldsymbol{x}}_{er} + \boldsymbol{K}_e\boldsymbol{x}_{er} + \boldsymbol{g}_e &= \boldsymbol{B}\boldsymbol{f}_r. \end{aligned} \tag{75}$$

Given the above equations and Eq. (47), the error dynamics is derived as follows:

$$\begin{aligned} \boldsymbol{M}_T\ddot{\tilde{\boldsymbol{x}}}_r + \boldsymbol{C}_T\dot{\tilde{\boldsymbol{x}}}_r &= \boldsymbol{f} - \boldsymbol{f}_r, \\ \boldsymbol{M}_e\ddot{\tilde{\boldsymbol{x}}}_e + \boldsymbol{D}_e\dot{\tilde{\boldsymbol{x}}}_e + \boldsymbol{K}_e\tilde{\boldsymbol{x}}_e &= \boldsymbol{B}(\boldsymbol{f} - \boldsymbol{f}_r), \end{aligned} \tag{76}$$

in which $\tilde{\boldsymbol{x}}_e$ is defined as $\tilde{\boldsymbol{x}}_e = \boldsymbol{x}_e - \boldsymbol{x}_{er}$.

Theorem 2 *Consider the cable driven robot represented by Eq.* (47). *The mapping of* $\boldsymbol{s}_\mu :\rightarrow (\boldsymbol{f} - \boldsymbol{f}_r)$ *is a passive relation.*

Proof Consider the following non-negative function:

$$V_\mu = \frac{1}{2}\dot{\tilde{\boldsymbol{x}}}_r^T\boldsymbol{M}_T\dot{\tilde{\boldsymbol{x}}}_r + \frac{1}{2}(1-\mu)(\dot{\tilde{\boldsymbol{x}}}_e^T\boldsymbol{M}_e\dot{\tilde{\boldsymbol{x}}}_e + \tilde{\boldsymbol{x}}_e^T\boldsymbol{K}_e\tilde{\boldsymbol{x}}_e), \tag{77}$$

in which $0 \leq \mu < 1$. Find the derivative of V_μ:

$$\begin{aligned} \dot{V}_\mu = {} & \dot{\tilde{\boldsymbol{x}}}_r^T(\boldsymbol{f} - \boldsymbol{f}_r - \boldsymbol{C}_T\dot{\tilde{\boldsymbol{x}}}_r) + \frac{1}{2}\dot{\tilde{\boldsymbol{x}}}_r^T\dot{\boldsymbol{M}}_T\dot{\tilde{\boldsymbol{x}}}_r + (1-\mu)\dot{\tilde{\boldsymbol{x}}}_e^T(\boldsymbol{B}(\boldsymbol{f} - \boldsymbol{f}_r) - \boldsymbol{D}_e\dot{\tilde{\boldsymbol{x}}}_e - \boldsymbol{K}_e\tilde{\boldsymbol{x}}_e) \\ & + (1-\mu)\tilde{\boldsymbol{x}}_e^T\boldsymbol{K}_e\dot{\tilde{\boldsymbol{x}}}_e, \end{aligned} \tag{78}$$

with some simplification and by using Eq. (74), one may have

$$\dot{V} = \boldsymbol{s}_\mu^T(\boldsymbol{f} - \boldsymbol{f}_r) - (1-\mu)\dot{\tilde{\boldsymbol{x}}}_e^T\boldsymbol{D}\dot{\tilde{\boldsymbol{x}}}_e. \tag{79}$$

Integrate the above equation:

$$\int_0^T \boldsymbol{s}_\mu^T(\boldsymbol{f} - \boldsymbol{f}_r)dt = V(T) - V(0) + (1-\mu)\int_0^T \dot{\tilde{\boldsymbol{x}}}_e^T\boldsymbol{D}_e\dot{\tilde{\boldsymbol{x}}}_e dt. \tag{80}$$

The above equation shows that, provided that $0 \leq \mu < 1$, there is a passive mapping between the input $(\boldsymbol{f} - \boldsymbol{f}_r)$ and the output $\boldsymbol{s}_\mu$. □

Therefore, we propose our control law as follows:

$$\boldsymbol{u} = \hat{\boldsymbol{J}}^\dagger \boldsymbol{f}_c + \alpha\boldsymbol{w}, \tag{81}$$

in which $\hat{\boldsymbol{J}}^\dagger$ is the pseudo-inverse of the estimated Jacobian, and $\boldsymbol{w}$ is a vector belonging to the null space of the Jacobian. Furthermore, α is a constant parameter used to perform an appropriate distribution of cable forces. In [27], the authors introduced a new method to select a proper α in practical implementations. In this paper, we use this proposed algorithm to guarantee positive forces in the robot cables. The parameter $\boldsymbol{f}_c$ is also derived:

$$\boldsymbol{f}_c = \hat{\boldsymbol{M}}_T\ddot{\boldsymbol{x}}_r + \hat{\boldsymbol{C}}_T\dot{\boldsymbol{x}}_r + \hat{\boldsymbol{g}}_T - \boldsymbol{K}_d\boldsymbol{s}_\mu. \tag{82}$$

Theorem 3 *Consider the dynamics of the cable driven robot represented by Eq.* (47). *In this system, the steady state value of* $\boldsymbol{s}_\mu$ *will remain uniformly ultimately bounded* (*UUB*) *as long as the value of* $\boldsymbol{K}_d$ *in Eq.* (82) *is sufficiently large.*

Proof According to the proposed control law described in Eq. (81), $\boldsymbol{f} - \boldsymbol{f}_r$ in Eq. (79) may be written as

$$\boldsymbol{f} - \boldsymbol{f}_r = \boldsymbol{J}^T \boldsymbol{u} - \boldsymbol{f}_r, \tag{83}$$

adding and subtracting $\boldsymbol{f}_c$ from the above equation and using the relation $\alpha \hat{\boldsymbol{J}}^T \boldsymbol{w} = 0$, we have

$$\begin{aligned} \boldsymbol{f} - \boldsymbol{f}_r &= \boldsymbol{J}^T (\hat{\boldsymbol{J}}^\dagger \boldsymbol{f}_c + \alpha \boldsymbol{w}) + \boldsymbol{f}_c - \boldsymbol{f}_c - \alpha \hat{\boldsymbol{J}}^T \boldsymbol{w} - \boldsymbol{f}_r \\ &= (\boldsymbol{J}^T \hat{\boldsymbol{J}}^\dagger - I) \boldsymbol{f}_c + \alpha (\boldsymbol{J}^T - \hat{\boldsymbol{J}}^T) \boldsymbol{w} + \boldsymbol{f}_c - \boldsymbol{f}_r. \end{aligned} \tag{84}$$

Substituting Eq. (82) in the above equation, $\boldsymbol{f} - \boldsymbol{f}_r$ can be formulated:

$$\boldsymbol{f} - \boldsymbol{f}_r = -\boldsymbol{K}_d \boldsymbol{s}_\mu + \rho, \tag{85}$$

where ρ encapsulates the system uncertainty and may be derived as

$$\rho = \tilde{\boldsymbol{M}}_T \ddot{\boldsymbol{x}}_r + \tilde{\boldsymbol{C}}_T + \tilde{\boldsymbol{g}} + (\boldsymbol{J}^T \hat{\boldsymbol{J}}^\dagger - I) \boldsymbol{f}_c + \alpha (\boldsymbol{J}^T - \hat{\boldsymbol{J}}^T) \boldsymbol{w}, \tag{86}$$

in which $\tilde{\boldsymbol{M}}_T = \hat{\boldsymbol{M}}_T - \boldsymbol{M}_T$, $\tilde{\boldsymbol{C}}_T = \hat{\boldsymbol{C}}_T - \boldsymbol{C}_T$ and $\tilde{\boldsymbol{g}}_T = \hat{\boldsymbol{g}}_T - \boldsymbol{g}_T$. Now, substitute Eq. (85) in Eq. (79):

$$\dot{V} = \boldsymbol{s}_\mu^T (\rho - \boldsymbol{K}_d \boldsymbol{s}_\mu) - (1 - \mu) \dot{\tilde{\boldsymbol{x}}}_e^T \boldsymbol{D} \dot{\tilde{\boldsymbol{x}}}_e. \tag{87}$$

Assume that the norm of the uncertainty $\|\rho\|_2$ is bounded by

$$\|\rho\|_2 < a_1 + a_2 \|\boldsymbol{s}_\mu\|_2, \tag{88}$$

in which a_1 and a_2 are positive constants, then

$$\dot{V} < -(\lambda_{\min}(\boldsymbol{K}_d) - a_2) \|\boldsymbol{s}_\mu\|^2 - (1 - \mu) \lambda_{\min}(\boldsymbol{D}) \|\dot{\tilde{\boldsymbol{x}}}_e\|^2 + a_1 \|\boldsymbol{s}_\mu\|. \tag{89}$$

Thus, the derivative of the proposed Lyapunov function is negative if $\|\boldsymbol{s}_\mu\|$ satisfies the following constraint:

$$\|\boldsymbol{s}_\mu\| > \frac{a_1}{\lambda_{\min}(\boldsymbol{K}_d) - a_2}. \tag{90}$$

In other words, the proposed controller can stabilize the robot if the controller gain $\boldsymbol{K}_d$ is set sufficiently large, and the error will remain UUB. □

6 Experimental results

In this section, a circular path is designed for the experiments, and the robot performance is verified on this path. This circular path has a radius of 40 cm, along which the robot travels four times in 25 seconds. To achieve a smooth motion along the path, this trajectory is designed such that the velocity at the beginning is zero, and it gradually increases. Furthermore, at the end of the path, the robot speed is gradually reduced to zero. In this experiment,

Table 1 Selected Values for The Control Parameters

Controller parameters	Values
Λ	$diag(10, 10, 10)$
$\boldsymbol{K}_d$	$diag(200, 200, 200)$

the weight of the end-effector is 4.5 kg, which is very high in comparison to the weight of the cables.

Using this trajectory and applying the controller law proposed in Eq. (81), the tracking performance is investigated in detail. In order to measure the effectiveness of the parameter μ, three experiments are designed, and in each test, the control law proposed in Eq. (81) is applied to the robot with a specific value for μ. In the first experiment, μ is set to zero and the redefined output of the system is measured. In this case, according to Eq. (56), the only feedback used to control and track the position of the end-effector is through the encoders. Therefore, the trajectory tracking error is expected to be high. Since data from the camera is not used in the feedback, and due to the kinematic uncertainties of the robot and the cable dynamics, the position obtained from the forward kinematic equations and the encoders would not be accurate. However, as can be seen from Eq. (56), by reduction of μ, the robot's stability and robustness improve.

In the second experiment, the design parameter μ is selected as $\mu = 0.4$. We expect the tracking performance to improve as μ is increased, since the control law uses camera data in the feedback. However, with the increase of μ, the robot stability becomes precarious, and the robot approaches the passivity boundary. Finally, and in the last experiment, $\mu = 0.8$ is considered. Because the control law is heavily dependent on camera data, the robot's accuracy is expected to significantly increase, but the smoothness of the motion of the robot is impaired.

6.1 Gain tuning methodology

One of the most critical parameters of the designed controller is the selection of the parameter μ. As explained before, if the intended use of the robot is such that tracking accuracy is important, then μ should be selected as large as possible. However, in applications such as the spider camera where the robot accuracy is not as important as the stability and smoothness of its motion, μ shall be set to a smaller value and closer to zero. The proper selection of the controller gains $\boldsymbol{K}_d$ and the parameters Λ in Eqs. (82) and (69) plays an important role in improving the robot tracking performance. As it is shown in the stability proof, increasing $\boldsymbol{K}_d$ improves the robot's stability and the tracking error is reduced. However, due to the presence of measurement noise and limitations on the sampling rate of the sensors, the parameter $\boldsymbol{K}_d$ cannot be selected too large. Furthermore, the variable Λ, which determines the ratio of position error to velocity error at the sliding surface, should be selected properly. Selecting small values for the parameter Λ allows for accurate tracking. In this case, the position error is more important than the speed error, choosing large values can lead to robot instability. Table 1 shows the final values selected for these control parameters.

6.2 Experimental results

Figure 5 shows the trajectory tracking performance for all three tests. As it is shown in this figure, the trajectory consists of four circular paths in the $x - y$ plane, which is tracked by

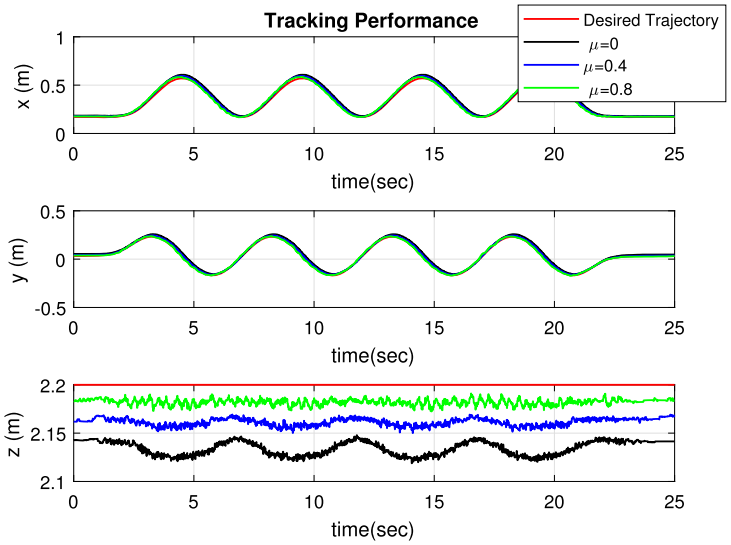

Fig. 5 The trajectory tracking of the proposed controller for different μ

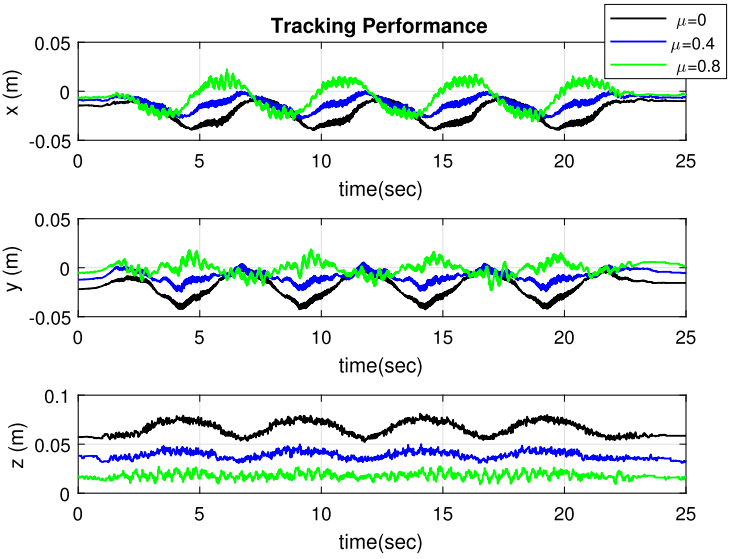

Fig. 6 The tracking error of the proposed controller for different μ

all three controllers. Figure 6 shows a close up of the tracking error in the three axes for the three controllers. As it is seen in these figures, when $\mu = 0.8$, the desired trajectory tracking is performed with higher accuracy as expected, since the weight of the stereo camera sensor in the feedback, in this case, is higher than that of the encoders. In contrast, Fig. 5 shows that, when μ is set to zero, the worst tracking accuracy of the robot is obtained. However, Fig. 6 shows that in this case, the undesirable vibration of the end-effector is reduced. Con-

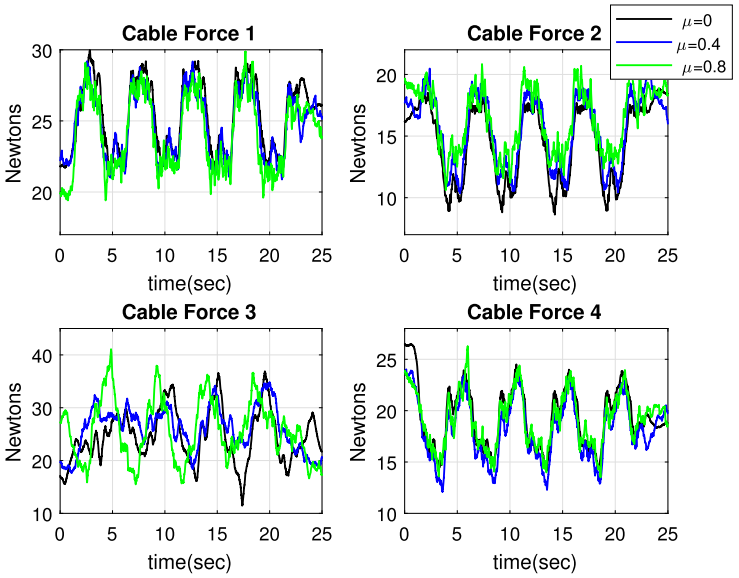

Fig. 7 The measured cable forces for different μs

Fig. 8 The circles traveled by the robot for different μs

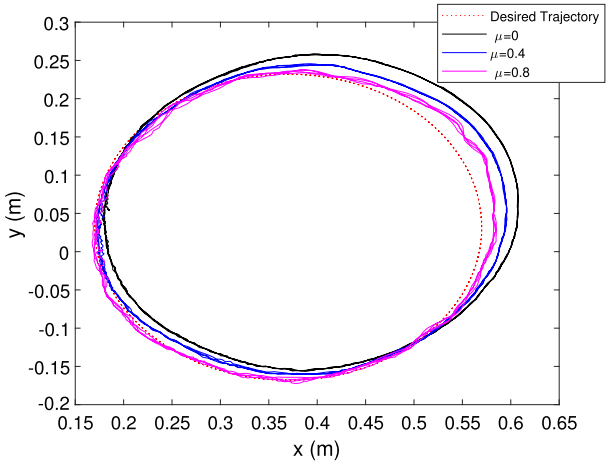

versely, when a larger gain for μ is selected, the end-effector oscillations occur with higher amplitudes and lower frequencies.

Figure 7 shows the measured cable forces for different controllers. As shown in Fig. 7, the drastic changes of cable forces are greater when a larger μ is selected. In other words, by choosing a smaller μ, the force adjustments in the cables are much smoother. Figure 8 shows better than the other figures the effect of the μ selection on the efficiency of the control algorithm. In this figure, the circular motion of the end-effector for various controllers is shown on the x–y plane. As shown in Fig. 8, when μ is equal to zero, the measured trajectory is far from the desired circle. In this case, the robot moves smoothly and without oscillation such that the four circles are perfectly aligned, and only one circle is seen in the figure. This

Table 2 Tracking error comparison table

	$e_x(m)$	$e_y(m)$	$e_z(m)$	$e_{total}(m)$
$\mu = 0$	0.0232	0.0216	0.066	0.042
$\mu = 0.4$	0.010	0.008	0.029	0.018
$\mu = 0.8$	0.006	0.003	0.014	0.009

shows that the robot performs well from the point of view of repeatability. In contrast, when $\mu = 0.8$, the absolute accuracy of the robot has increased, but in this case, the circles do not coincide. This is because of undesirable oscillations of the end-effector, which occur more frequently in this case, hindering the overall repeatability. Finally, it can be concluded that in order to achieve optimal robot performance, a trade-off is needed between the robot tracking error and the undesirable oscillations. Table 2 shows the root mean square error of tracking for different values of μ. As indicated in this table by increasing μ, the tracking error decreases from 0.042 to 0.009. However, as mentioned earlier, this increase in the robot accuracy is achieved at the cost of increasing the end-effector oscillations

7 Conclusions

In this paper, a robot dynamic model based on a lumped mass representation of the cables was presented along with a control algorithm ensuring the robot stability in the presence of kinematic and dynamic uncertainty. The proposed robot control algorithm was designed based on the passivity method, and it is shown that combining the camera and encoder data can produce adequate results. The theoretical and practical results showed that the more the algorithm relies on encoder data, the more robust is the robot motion. On the contrary, as the weight of the camera's data in the data fusion process increases, the system approaches the passivity boundary and becomes unstable. It is shown that, according to the robot application, making a trade-off between the efficiency and the robustness of the control system is necessary. Finally, it is determined that $\mu = 0.4$ is an appropriate setting for the ARAS–CAM, as the robot's motion is then accurate, while exhibiting very little oscillation.

Acknowledgements The authors appreciate the support from Iranian National Science Foundation (INSF) under grant number 96001803.

References

1. Taghirad, H.: Parallel Robots: Mechanics and Control. Taylor & Francis, London (2012)
2. Behzadipour, S., Khajepour, A.: A new cable-based parallel robot with three degrees of freedom. Multibody Syst. Dyn. **13**(4), 371–383 (2005)
3. Khalilpour, S., Khorrambakht, R., Taghirad, H., Cardou, P.: Wave based control of a deployable cable driven robot. In: 2018 6th RSI International Conference on Robotics and Mechatronics (IcRoM), pp. 166–171. IEEE Press, New York (2018)
4. Jordan, B.L., Batalin, M.A., Kaiser, W.J.: Nims rd: a rapidly deployable cable based robot. In: Proceedings 2007 IEEE International Conference on Robotics and Automation, pp. 144–150. IEEE Press, New York (2007)
5. Borgstrom, P.H., Jordan, B.L., Borgstrom, B.J., Stealey, M.J., Sukhatme, G.S., Batalin, M.A., Kaiser, W.J.: Nims-pl: a cable-driven robot with self-calibration capabilities. IEEE Trans. Robot. **25**(5), 1005–1015 (2009)

6. Bosscher, P., Williams, R.L., Tummino, M.: A concept for rapidly-deployable cable robot search and rescue systems. In: ASME 2005 International Design Engineering Technical Conferences and Computers and Information in Engineering Conference, pp. 589–598. American Society of Mechanical Engineers, New York (2005)
7. Merlet, J.: Marionet, a family of modular wire-driven parallel robots. In: Advances in Robot Kinematics: Motion in Man and Machine, pp. 53–61 (2010)
8. Cheah, C.C., Kawamura, S., Arimoto, S.: Feedback control for robotic manipulator with an uncertain Jacobian matrix. J. Robot. Syst. **16**(2), 119–134 (1999)
9. Cheah, C.C., Hirano, M., Kawamura, S., Arimoto, S.: Approximate Jacobian control for robots with uncertain kinematics and dynamics. IEEE Trans. Robot. Autom. **19**(4), 692–702 (2003)
10. Khalilpour, S., Khorrambakht, R., Harandi, M., Taghirad, H., Cardou, P.: Cascade terminal sliding mode control of a deployable cable driven robot. In: 2019 6th International Conference on Control, Instrumentation and Automation (ICCIA), pp. 1–6. IEEE Press, New York (2019)
11. Procházka, F., Valášek, M., Šika, Z.: Robust sliding mode control of redundantly actuated parallel mechanisms with respect to geometric imperfections. Multibody Syst. Dyn. **36**(3), 221–236 (2016)
12. Gorman, J.J., Jablokow, K.W., Cannon, D.J.: The cable array robot: theory and experiment. In: Proceedings 2001 ICRA. IEEE International Conference on Robotics and Automation (Cat. No. 01CH37164), vol. 3, pp. 2804–2810. IEEE Press, New York (2001)
13. Oh, S.R., Agrawal, S.K.: Cable suspended planar robots with redundant cables: controllers with positive tensions. IEEE Trans. Robot. **21**(3), 457–465 (2005)
14. Oh, S.R., Agrawal, S.K.: Generation of feasible set points and control of a cable robot. IEEE Trans. Robot. **22**(3), 551–558 (2006)
15. Khalilpour, S., Khorrambakht, R., Taghirad, H., Cardou, P.: Cascade control of a deployable cable–driven robot with elastic cables. IEEE Trans. Syst. Man Cybern. Syst. (2020, submitted)
16. Begey, J., Cuvillon, L., Lesellier, M., Gouttefarde, M., Gangloff, J.: Dynamic control of parallel robots driven by flexible cables and actuated by position-controlled winches. IEEE Trans. Robot. **35**(1), 286–293 (2018)
17. Diao, X., Ma, O.: Vibration analysis of cable-driven parallel manipulators. Multibody Syst. Dyn. **21**(4), 347–360 (2009)
18. Khalilpour, S., Khorrambakht, R., Taghirad, H., Cardou, P.: Dual space control of a deployable cable driven robot: wave based approach. Int. J. Soc. Robot. Theory Appl. **6**(1), 11–19 (2020)
19. Rushton, M., Khajepour, A.: Transverse vibration control in planar cable-driven robotic manipulators. In: Cable-Driven Parallel Robots, pp. 243–253. Springer, Berlin (2018)
20. de Rijk, R., Rushton, M., Khajepour, A.: Out-of-plane vibration control of a planar cable-driven parallel robot. IEEE/ASME Trans. Mechatron. **23**(4), 1684–1692 (2018)
21. Jamshidifar, H., Khosravani, S., Fidan, B., Khajepour, A.: Vibration decoupled modeling and robust control of redundant cable-driven parallel robots. IEEE/ASME Trans. Mechatron. **23**(2), 690–701 (2018)
22. Babaghasabha, R., Khosravi, M.A., Taghirad, H.D.: Adaptive robust control of fully constrained cable robots: singular perturbation approach. Nonlinear Dyn. **85**, 607–620 (2016)
23. Caverly, R.J., Forbes, J.R., Mohammadshahi, D.: Dynamic modeling and passivity-based control of a single degree of freedom cable-actuated system. IEEE Trans. Control Syst. Technol. **23**(3), 898–909 (2014)
24. Caverly, R.J., Forbes, J.R.: Dynamic modeling and noncollocated control of a flexible planar cable-driven manipulator. IEEE Trans. Robot. **30**(6), 1386–1397 (2014)
25. Walton, T.S., Polachek, H.: Calculation of transient motion of submerged cables. Math. Comput. **14**(69), 27–46 (1960)
26. Nagatomi, O., Nakamura, M., Koterayama, W., et al.: Dynamic simulation and field experiment of submarine cable during laying and recovery. In: The Twelfth International Offshore and Polar Engineering Conference. International Society of Offshore and Polar Engineers, Mountain View (2002)
27. Khalilpour, S., Khorrambakht, R., Taghirad, H., Cardou, P.: Robust cascade control of a deployable cable-driven robot. Mech. Syst. Signal Process. **127**, 513–530 (2019)
28. Khalilpour, S., Khorrambakht, R., Bourbour, A., Taghirad, H.: Joint-space position control of a deployable cable driven robot in joint space using force sensors and actuator encoders. Modares Mech. Eng. **19**(11), 2615–2625 (2019)
29. Hosseini, M.I., Harandi, M.J., Seyedi, S.A.K., et al.: Adaptive fast terminal sliding mode control of a suspended cable-driven robot. In: 2019 27th Iranian Conference on Electrical Engineering (ICEE), pp. 985–990. IEEE Press, New York (2019)
30. Damaren, C.J.: Passivity analysis for flexible multilink space manipulators. J. Guid. Control Dyn. **18**(2), 272–279 (1995)
31. Damaren, C.J.: On the dynamics and control of flexible multibody systems with closed loops. Int. J. Robot. Res. **19**(3), 238–253 (2000)

32. Damaren, C.J.: Adaptive control of flexible manipulators carrying large uncertain payloads. J. Robot. Syst. **13**(4), 219–228 (1996)
33. Damaren, C.: Approximate inverse dynamics and passive feedback for flexible manipulators with large payloads. IEEE Trans. Robot. Autom. **12**(1), 131–138 (1996)
34. Spector, V., Flashner, H.: Sensitivity of structural models for noncollocated control systems. J. Dyn. Syst. Meas. Control **111**(4), 646–655 (1989)
35. Spector, V., Flashner, H.: Modeling and design implications of noncollocated control in flexible systems. J. Dyn. Syst. Meas. Control **112**(2), 186–193 (1990)
36. Miu, D.K.: Physical interpretation of transfer function zeros for simple control systems with mechanical flexibilities. J. Dyn. Syst. Meas. Control **113**(3), 419–424 (1991)
37. Wang, D., Vidyasagar, M.: Passive control of a single flexible link. In: Proceedings., IEEE International Conference on Robotics and Automation, pp. 1432–1437. IEEE Press, New York (1990)
38. Pota, H.R., Vidyasagar, M.: Passivity of flexible beam transfer functions with modified outputs. In: Proceedings, 1991 IEEE International Conference on Robotics and Automation, pp. 2826–2831. IEEE Press, New York (1991)
39. Desoer, C.A., Vidyasagar, M.: Feedback Systems: Input-Output Properties, vol. 55. SIAM, Philadelphia (1975)
40. Damaren, C.J.: Modal properties and control system design for two-link flexible manipulators. Int. J. Robot. Res. **17**(6), 667–678 (1998)